

2-1770


UCRL-JC-127168  
PREPRINT

## **Cryogenic, High-Resolution X-ray Spectrometers for SR-XRF and Microanalysis**

**M. Frank, C. A. Mears, S. E. Labov, L. J. Hiller, J. B. le Grand,  
M. A. Lindeman, H. Netel, D. Chow, A. T. Barfknecht**

**This paper was prepared for submittal to the  
Synchrotron Radiation Instrumentation Conference  
Himeji, Japan  
August 4-8, 1997**

**October 30, 1997**



**Lawrence  
Livermore  
National  
Laboratory**

**This is a preprint of a paper intended for publication in a journal or proceedings. Since changes may be made before publication, this preprint is made available with the understanding that it will not be cited or reproduced without the permission of the author.**

#### DISCLAIMER

This document was prepared as an account of work sponsored by an agency of the United States Government. Neither the United States Government nor the University of California nor any of their employees, makes any warranty, express or implied, or assumes any legal liability or responsibility for the accuracy, completeness, or usefulness of any information, apparatus, product, or process disclosed, or represents that its use would not infringe privately owned rights. Reference herein to any specific commercial product, process, or service by trade name, trademark, manufacturer, or otherwise, does not necessarily constitute or imply its endorsement, recommendation, or favoring by the United States Government or the University of California. The views and opinions of authors expressed herein do not necessarily state or reflect those of the United States Government or the University of California, and shall not be used for advertising or product endorsement purposes.

# **Cryogenic, High-Resolution X-ray Spectrometers for SR-XRF and Microanalysis**

**M. Frank\*, C.A. Mears, S.E. Labov, L.J. Hiller, J.B. le Grand,  
M.A. Lindeman, H. Netel, D. Chow**  
*Lawrence Livermore National Laboratory,  
P.O. Box 808, L-401, Livermore CA 94551, USA*

**A. T. Barfknecht**  
*Conductus, Inc.,  
969 West Maude Ave., Sunnyvale, CA 94086, USA*

**October 30, 1997**

**Keywords:** Cryogenic Detectors, Low Temperature Detectors, Microcalorimeters, X-ray fluorescence, X-ray spectroscopy

## **Abstract**

We present experimental results obtained with a cryogenically-cooled, high-resolution X-ray spectrometer based on a  $141\ \mu\text{m} \times 141\ \mu\text{m}$  Nb-Al-Al<sub>2</sub>O<sub>3</sub>-Al-Nb superconducting tunnel junction (STJ) detector in an SR-XRF demonstration experiment. STJ detectors can operate at count rates approaching those of semiconductor detectors while still providing a significantly better energy resolution for soft X rays. Measuring fluorescence X rays from samples containing transition metals and low-Z elements we obtained a FWHM energy resolution of 6 - 15 eV for X rays in the energy range between 180 eV and 1100 eV. Our results show that in the near future STJ detectors may prove very useful in XRF and microanalysis applications.

\* corresponding author, email: matt@imager.llnl.gov, FAX: (510) 424-5512

to be submitted to Journal of Synchrotron Radiation, Proceedings of SRI'97

## 1. Introduction

Superconducting tunnel junctions (STJs) are one prominent type of cryogenic detectors, a new class of energy-resolving photon and particle detectors (Ott & Zehnder, 1996, Twerenbold, 1996, Booth & Goldie, 1996). The energy resolution of such detectors, typically operating at temperatures below  $\sim 1$  K, can be at least an order of magnitude better than for conventional, ionization-based semiconductor detectors such as SiLi or Ge detectors. Among the best reported photon energy resolutions achieved with STJ detectors are 29 eV (FWHM) at 6 keV (Mears, et al., 1996), 12.5 eV at 1 keV (Hiller, et al., 1995) and 1.3 eV at 3.5 eV (Peacock, et al., 1996). Compared to other types of cryogenic detectors STJ detectors can count at high count rates of several 10,000 counts per second (cps) because of their relatively fast ( $\sim \mu\text{s}$ ) pulse decay times. In addition, the cryogenics and electronics required for operating STJ detectors are relatively simple. These properties render STJ detectors potentially interesting tools for a wide range of applications such as X-ray fluorescence microanalysis or synchrotron radiation X-ray fluorescence.

In a previous paper (Frank, et al., 1997) we described the results of a detector performance study in which the STJ detector was irradiated *directly* with a monochromatized synchrotron beam. In that study we achieved an energy resolution of 5.9 eV (FWHM) for 277 eV X rays (the energy corresponding to C K) and an electronic noise of 4.5 eV at low count rates of several 100 cps. Increasing the count rate up to 10,000 cps, the energy resolution of our detector at an incident energy of 277 eV remained better than 10 eV. For higher count rates the resolution degraded slowly with increasing rate to 20 eV for 277 eV X rays at 50,000 cps. We also found that the intrinsic energy resolution for this detector for X-rays in the range between 70 and 700 eV scaled roughly linear with the incident energy. Here we present experimental results obtained using the same detector in a SR-XRF demonstration experiment also performed at SSRL in which we measured fluorescence X rays from samples containing transition metals and low-Z elements.

## 2. Experimental Details

Fig. 1 shows a schematic cross section (a) and a schematic top view (b) of the STJ detector, which was fabricated at Conductus, Inc., using a modified photolithographic Nb trilayer process (Barfknecht, et al., 1991). The detector consists of a 265 nm thick Nb base layer and a 165 nm thick Nb counter electrode separated by a thin ( $\sim 20$  Å)  $\text{Al}_2\text{O}_3$  tunnel

barrier with 50 nm thick Al "trapping" layers on each side. The detector is diamond-shaped with an area of  $141\ \mu\text{m} \times 141\ \mu\text{m}$ . During operation a small bias voltage ( $V_{\text{bias}} \sim 0.4\ \text{mV}$ ) is applied across the barrier. Also a small magnetic field ( $B \sim 100\ \text{Gauss}$ ) is applied parallel to the tunnel barrier and in the direction indicated in Fig. 1b in order to suppress the dc Josephson current in the device. The detector is operated at a temperature of 500 mK or below, which is well below the superconducting transition temperature of the superconducting layers. The absorption of an X-ray photon in one of the layers breaks Cooper pairs in the superconductor creating quasiparticle excitations, which can quantum-mechanically tunnel through the  $\text{Al}_2\text{O}_3$  barrier and create a measurable current pulse. The amplitude of the current pulse, typically fractions of a microampere, is proportional to the energy of the absorbed X-ray photon. The current pulse decay time is typically given by the quasiparticle life time of a few microseconds. The Al layers with lower superconducting gap energy than the Nb layers help increasing the signal by concentrating quasiparticles near the tunnel barrier by means of "quasiparticle trapping" (Booth, 1987). For more details on the operating principle see (Mears, et al., 1995, Frank, et al., 1997). The theoretical limit for the FWHM energy resolution of an X-ray spectrometer based on the measurement of the X-ray induced quasiparticle excitations in pure Nb has been calculated to be about 5 eV at 6 keV incident X-ray energy (Rando, et al., 1992). In practice, additional statistical fluctuations associated with the trapping, tunneling and recombination processes (Mears, et al., 1993, Goldie, et al., 1994) may degrade this limit, but a resolution of  $\sim 10\ \text{eV}$  at 6 keV should be obtainable.

A schematic of the experimental setup is shown in Fig. 2. The STJ detector was housed in a pumped liquid helium cryostat equipped with an adiabatic demagnetization refrigerator (ADR) unit with a base temperature of  $\sim 50\ \text{mK}$ . The detector was attached to a cold stage in good thermal contact with the ADR unit. During the experiments the ADR temperature was *not* regulated and allowed to drift up freely to  $\sim 500\ \text{mK}$ , at which point the detector performance started to degrade. Typically this drift occurred over a period of  $\sim 4$  hours. After that, the ADR unit had to be recycled, i.e., run through a magnetization-demagnetization cycle, which typically took about 20 minutes. The fluorescence sample was located on the tip of a sample holder arm which could be inserted into the cryostat and placed into the synchrotron beam through a load lock system. During the measurements this tip was heat sunk to the 2 K stage of the cryostat. The load lock system allowed us to change samples in about  $\sim 30$  minutes. The distance between the sample and the detector was  $\sim 1.5\ \text{cm}$ . A thin window consisting of  $1000\ \text{\AA}$  parylene and  $200\ \text{\AA}$  aluminum in front of the detector was used to block Auger electrons.

We used a FET-based preamplifier with fast ( $\sim 500$  ns) negative feedback to measure the current signal from the STJ detector. The rise time of the current pulses was limited by this amplifier to typically  $\sim 500$  ns, the decay time of the current pulses was about  $4\text{--}5$   $\mu\text{s}$ . The pulses were further amplified and shaped with a simple band pass filter and then fed into a pulse height analyzer without any further signal processing. The measurements reported here were performed at relatively low count rates of  $\sim 1000$  cps to obtain optimal energy resolution. Above  $\sim 1000$  cps a slight degradation of the resolution could be observed. During most measurements we also injected pulses with similar shape from a pulse generator into the electronics to monitor the electronic noise.

### 3. Results

Fig. 3 shows the X-ray fluorescence spectrum obtained with a sample consisting of boron nitride covered partially with titanium powder excited by  $500$  eV X rays. This sample was chosen to simulate B and TiN, which are important materials in semiconductor fabrication. The K lines of B, N and the L line of Ti are well separated in this spectrum. Also present in this spectrum are K lines from C and O, presumably from oxides and contaminations in the sample and an X-ray line at  $500$  eV from scattered incident X rays. The FWHM energy resolution of the X-ray lines ranges from  $9.6$  eV for C K to  $13.1$  eV for Ti L. The electronic noise in this measurement was  $6.7$  eV as indicated by the width of the pulser line. For comparison, the resolution of SiLi detectors in this energy range is about a factor 10 worse and not sufficient to separate the Ti L line from N K.

The K lines of B, C and N in Fig. 4 are each accompanied by a "hump" of events at the low-energy side of the line labeled "surface layer events." These humps were also found during previous measurements, in which the detector was irradiated directly with the synchrotron beam (Frank, 1997). They probably originate from events caused by X-rays absorbed in a less responsive surface layer of our detector. Such a surface layer may be composed of niobium oxide, residues of  $\text{SiO}_2$  from the detector fabrication process or other surface contaminations and predominantly affects the lower energy X rays. The exact origin of these surface layer events and the other background seen at the low-energy end of the spectrum is still under study.

Fig. 4 shows a fluorescence spectrum measured with a manganese oxide sample and an incident beam energy of 700 eV. The Mn L lines are well resolved from the large O K line. Other X-ray lines present in this spectrum are Na K and F K which are probably due to contamination of the sample, Cu K from fluorescence of cryostat parts made of copper and C X rays which may originate in the parylene Auger electron blocking filter in front of the detector. The energy resolution in this spectrum ranges from 8.6 eV at C K to 16.1 eV at Na K. The electronic noise was 4.6 eV. An expanded part of this spectrum is shown in Fig. 5 revealing the Mn L lines in more detail. With the measured resolution of 11.2 eV at 640 eV the line splitting between Mn L  $\alpha$  and L  $\beta$  is visible. The ability to measure Mn fluorescence in the presence of large amounts of O is interesting for various biological studies, e.g. the study of photosystem II which is a protein containing Mn (Cramer, et al., 1992, Peng, et al., 1994). These measurements are very difficult with conventional detectors because of significant line overlap between O K and Mn L.

Fig. 6 shows part of a fluorescence spectrum measured with a sample from a magnetic storage disk fabricated by IBM with 1000 eV incident X rays. The composition and thickness of the various metal layers in this sample is indicated on the right side of this figure. Most of the L lines of the transition elements present in the sample (Cr, Co and Ni) are resolved from each other and indications for some substructures of the lines are visible. The resolution in the energy range shown was 10–15 eV.

#### 4. Conclusions

We have demonstrated the feasibility of performing SR-XRF measurements with a STJ detector cooled to ~100 mK in the environment of a room temperature synchrotron beam line. The measured detector resolution in the energy range from 100 - 1000 eV was 6-16 eV. Thus the K X-ray lines from the low-Z elements such as B, C, N, O, and F and transition element L lines in between could largely be resolved. The measurements reported here were performed at relatively low count rates of ~1000 cps to obtain the optimal energy resolution. We have recently shown that our detector can count at much higher rates up to several 10,000 cps with only moderate degradation of resolution. Thus STJ detectors can approach count rates possible with semiconductor detectors while still providing a significantly better energy resolution for soft X rays. These results indicate that STJ detectors may prove very useful in XRF and microanalysis applications studying light elements and transition metals.

## Acknowledgments

The authors would like to thank Jan Batteux, Dennis Carr, Steve Cramer, Jeff Moore, Pierro Pianetta, and the technical staff at SSRL for advice and expert technical support. We would also like to thank Brian York at IBM for providing samples. This work was performed under the auspices of the U.S. Department of Energy by Lawrence Livermore National Laboratory under contract no. W-7405-ENG-48 at the Stanford Synchrotron Radiation Laboratory (SSRL) which is operated by the Department of Energy, Office of Basic Energy Sciences under contract number is DE-AC03-76SF00515. This work was supported by NASA SBIR contract NAS5-32805 and NASA UV detector development grant NAGW 3907.

## References

- Barfknecht, A.T., Ruby, R.C. & Ko, H. (1991). IEEE Trans. Mag., **MAG-27**, 3125-3128.
- Booth, N.E. (1987). Appl. Phys. Lett. **50**, 293-295.
- Booth, N. E. & Goldie, D.J. (1996). Superconductor Science and Technology, **9**, 493-516.
- Cramer, S.P., Chen, J., George, S.J., Vanelp, J. and others (1992). Nucl. Instr. Meth. A **319**, 285-289.
- Frank, M., Mears, C.A., Labov, S.E., Hiller, L.J., le Grand, J.B., Lindeman, M.A., Netel, H., Chow, D., Caldara, G. & Barfknecht, A.T. (1997), submitted to Rev. Sci. Instr. June 1997.
- Goldie, D.J., Brink, P.L., Patel, C., Booth, N.E. & Salmon, G.L. (1994). Appl. Phys. Lett. **64**, 3169-3171.
- Hiller, L.J., Labov, S.E., Mears, C.A., Barfknecht, A.T., Frank, M., Netel, H. & Lindeman, M.A. (1995). "EUV, X-Ray and Gamma-Ray Instrumentation for Astronomy VI," Oswald H. W. Siegmund, John V, Vallergera, eds., Proc. SPIE **2518**, 249-255.
- Mears, C.A., Labov, S.E. & Barfknecht, A.T. (1993). Appl. Phys. Lett. **63**, 2961-2963.
- Mears, C.A., Labov, S.E., Hiller, L.J., Frank, M., Netel, H. Azgui, F. & Barfknecht, A.T. (1995). IEEE Trans. Appl. Supercond. **5**, 3069-3072.
- Mears, C.A., Labov, S.E., Frank, M., Lindeman, M.A., Hiller, L.J., Netel, H. & Barfknecht, A.T. (1996). Nucl. Instr. Meth. A. **370**, 53-56.



- Ott, H.R. & Zehnder, A. eds. (1996). Proceedings of the 6th International Workshop on Low Temperature Detectors, Beatenberg, Switzerland, August 1995, Nucl. Instr. Meth. A **370**, No. 1., 1-300.
- Peacock, A. (1996). A. Peacock, P. Verhoeve, N. Rando, A. van Dordrecht, B.G. Taylor, C. Erd, M.A.C. Perryman, R. Venn, J. Howlett, D.J. Goldie, J. Lumley, and M. Wallis, Nature, **381**, 135-137.
- Peng, G., Degroot, F.M.F., Hamalainen, K., Moore, J.A., and others (1994). J. Am. Chem. Soc. **116**, 2914-2920.
- Rando, N., Peacock, A., van Dordrecht, A., Foden, C. L., Engelhardt, R., Taylor, B. G., Gare, P. Lumley, J. & Pereira, C. (1992). Nucl. Instr. Meth. **313**, 173-195.
- Twerenbold, D. (1996). Rep. Progr. Part. Phys, **59**, 349-426.

## Figure Captions

**Fig. 1:** A schematic cross section of the STJ detector. The detector is diamond-shaped with an area of  $141\text{ }\mu\text{m} \times 141\text{ }\mu\text{m}$ . This detector was fabricated at Conductus, Inc., using a modified photolithographic Nb trilayer process.

**Fig. 2:** Schematic of the experimental setup as discussed in the text.

**Fig. 3:** Fluorescence spectrum obtained with a sample consisting of boron nitride covered partially with titanium powder excited by 500 eV X rays. The FWHM energy resolution ranges from 9.6 eV for C K to 13.1 eV for Ti L. The electronic noise was 6.7 eV.

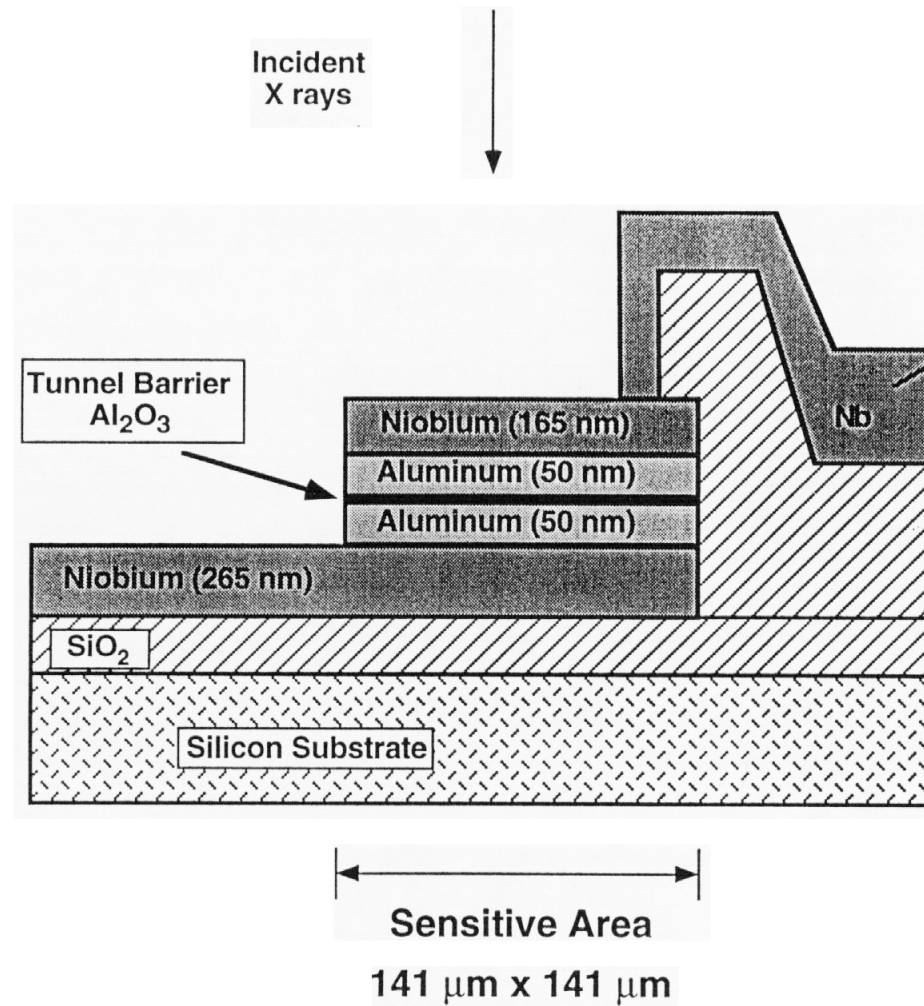
**Fig. 4:** Fluorescence spectrum with a manganese oxide sample and an incident beam energy of 700 eV. The Mn L lines are well resolved from the large O K line. Na K and F K are probably due to contamination of the sample, Cu K and C K may originate from parts of the cryostat exposed to the incident beam. The numbers indicate the FWHM energy resolution. The electronic noise was 4.6 eV.

**Fig. 5:** An expanded part of the spectrum from Fig. 4 containing revealing the Mn L lines in more detail.

**Fig. 6:** Fluorescence spectrum measured with a sample from a magnetic storage disk fabricated by IBM with 1000 eV incident X rays. The composition and thickness of the

various metal layers in this sample is indicated on the right side of this figure. The energy resolution in the energy range shown was 10–15 eV.

a) cross section



b) top view

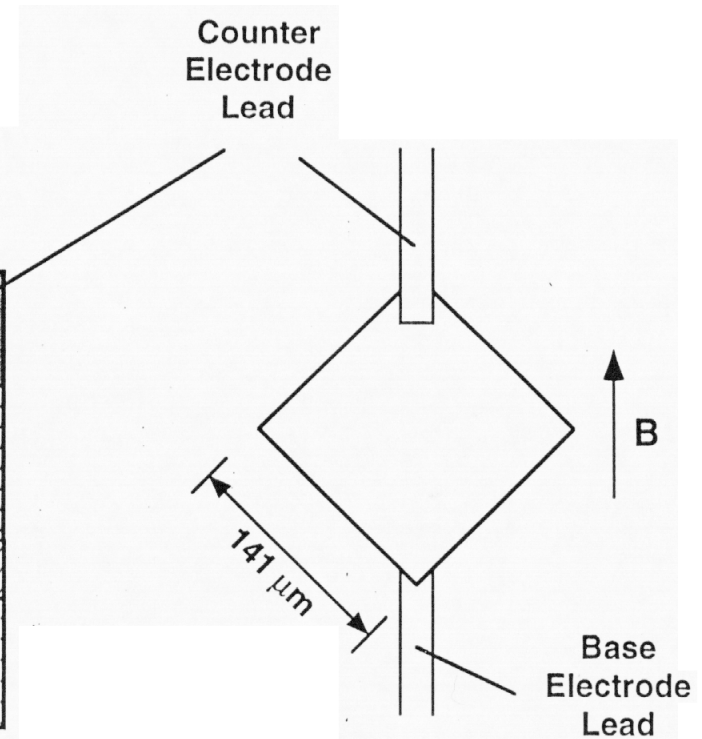


Fig. 1, M. Frank

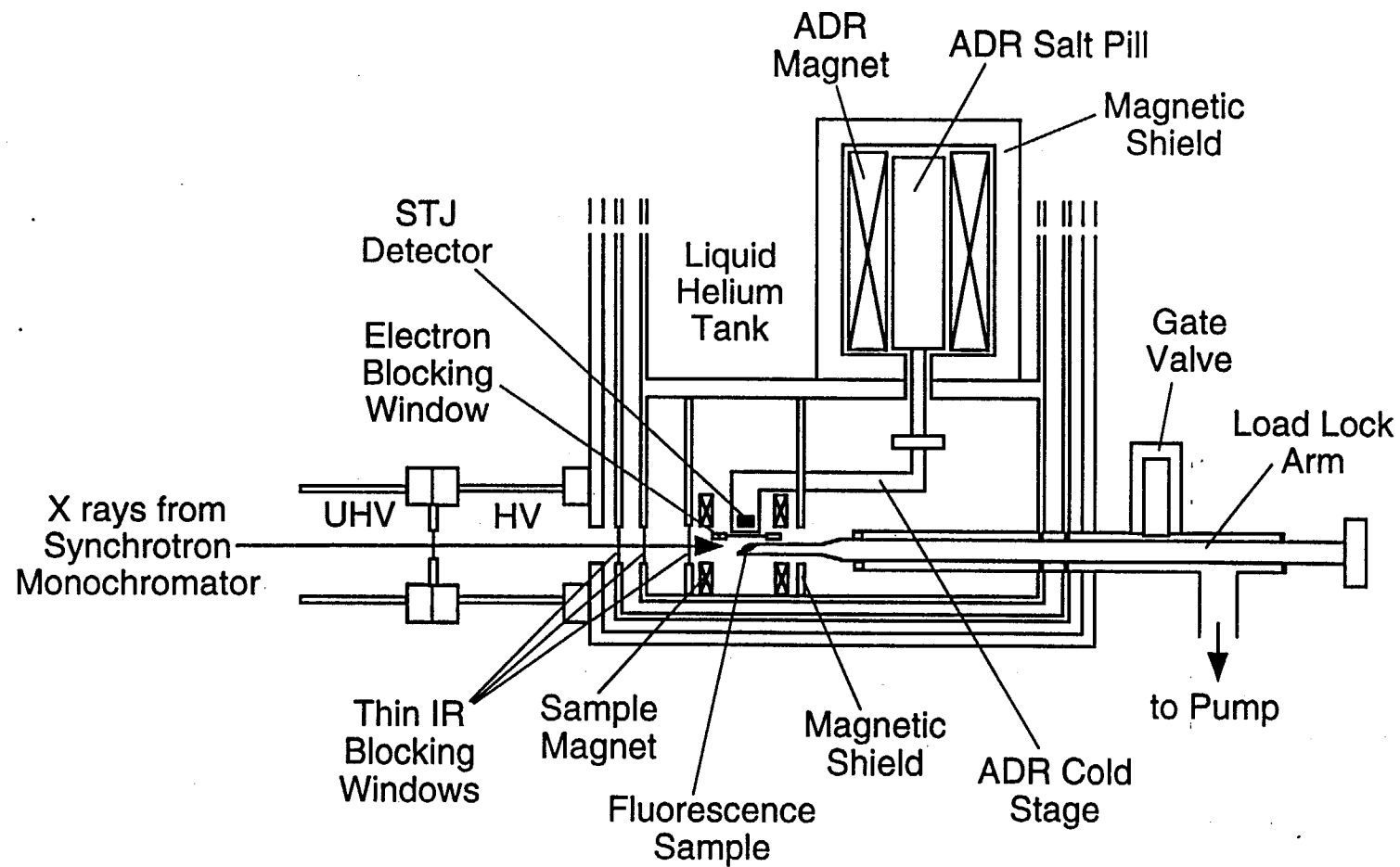


Fig. 2, M. Frank

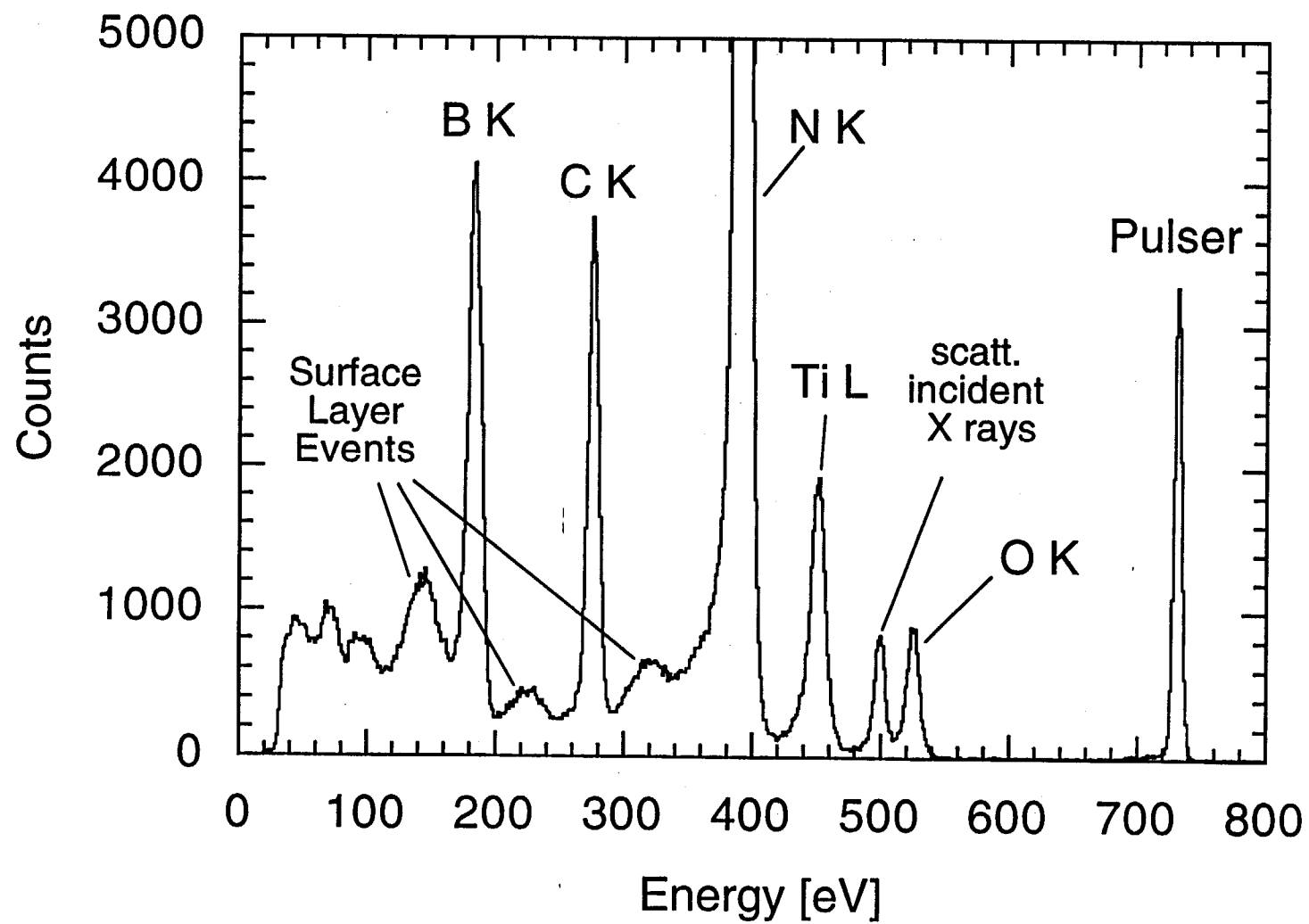


Fig. 3, M. Frank

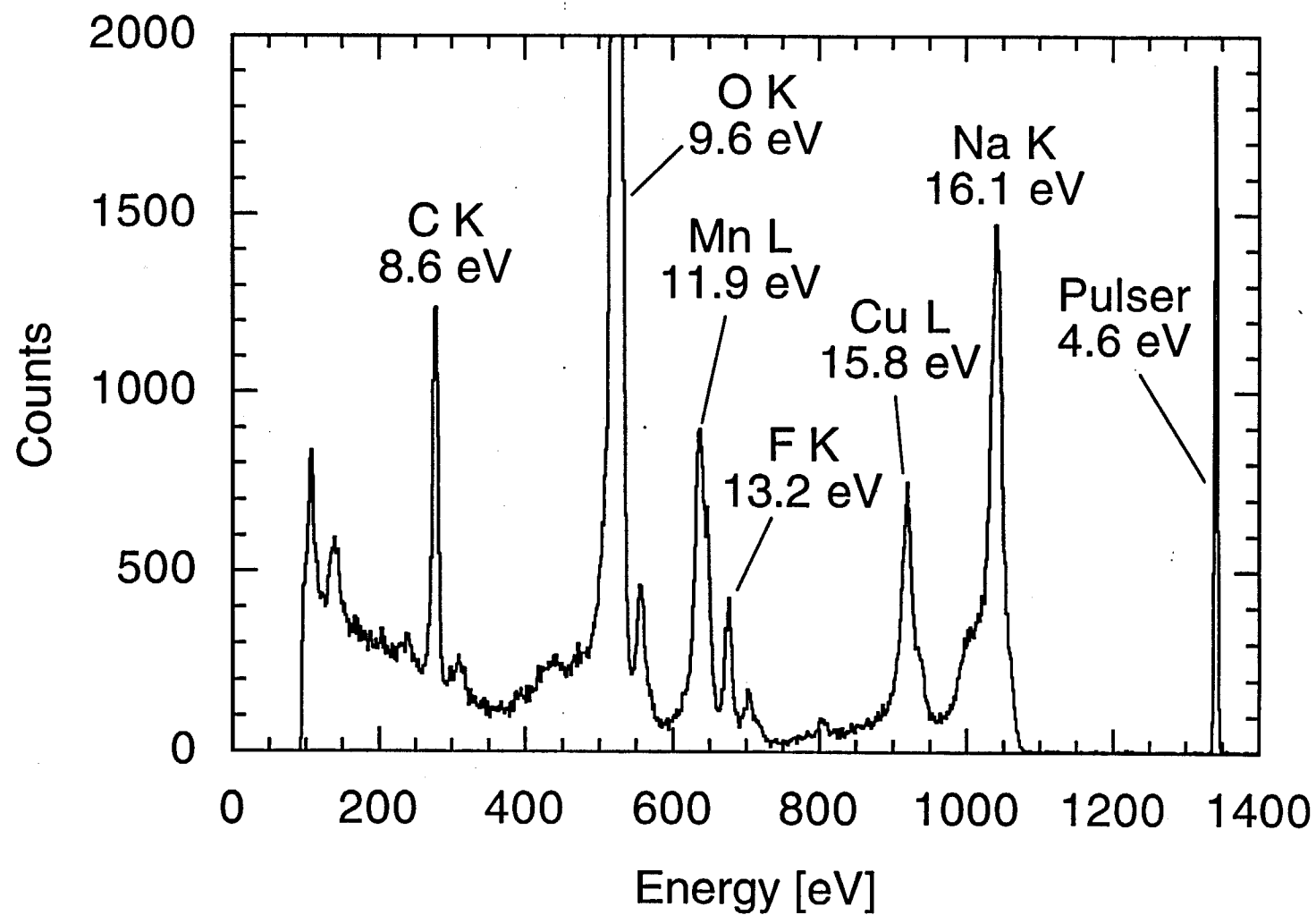


Fig. 4, M. Frank

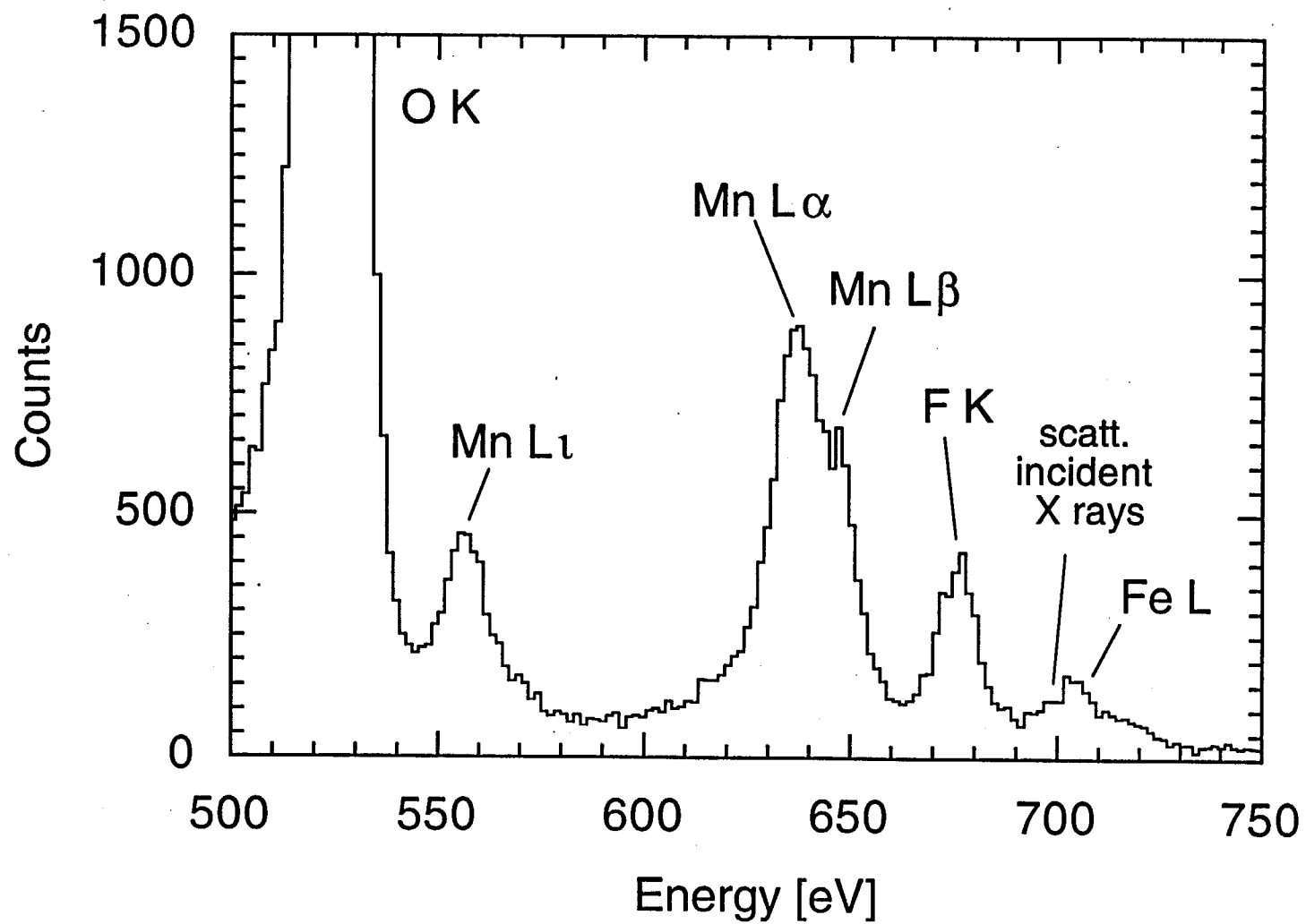


Fig. 5, M. Frank

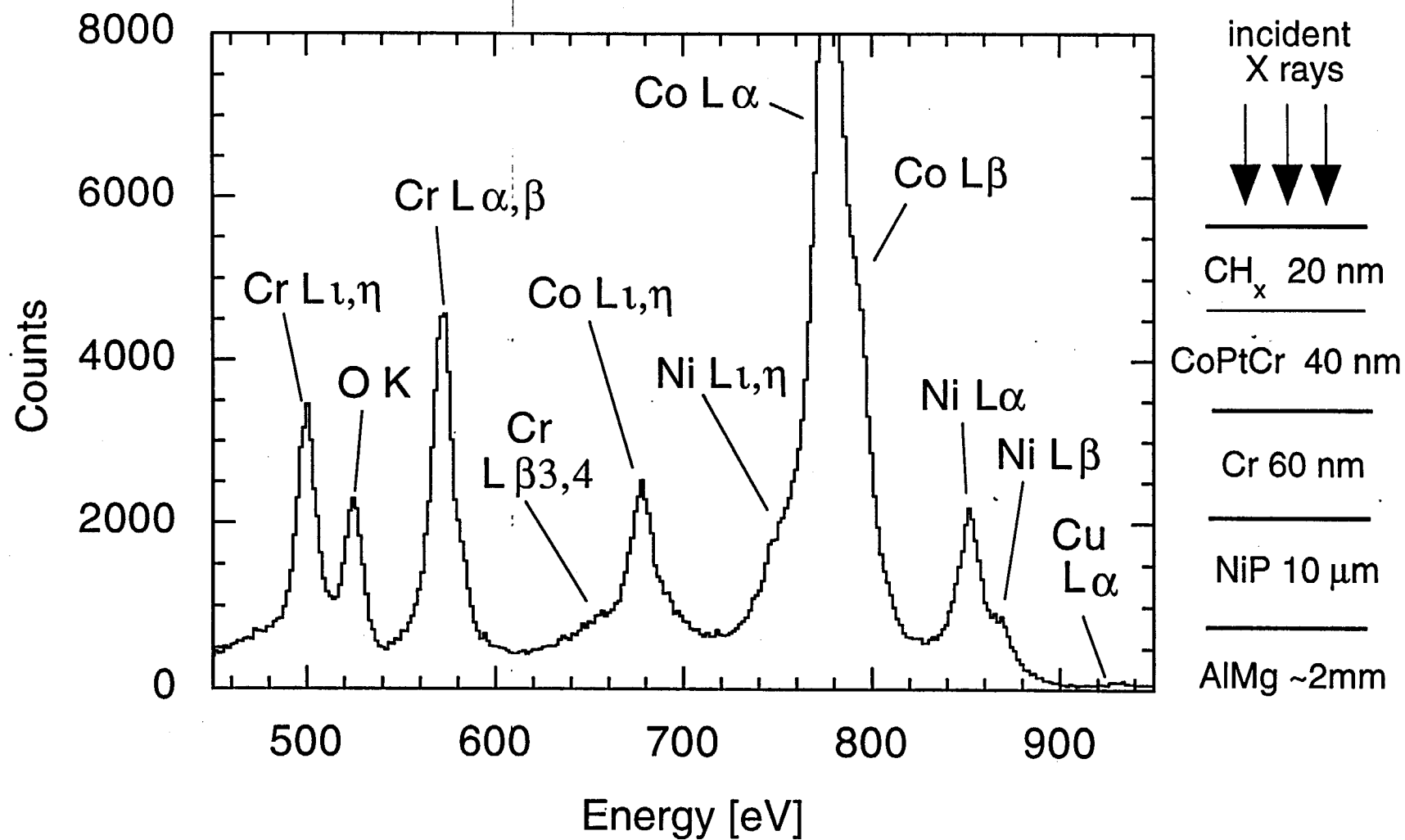


Fig. 6, M. Frank